

# Angular clustering of point sources at 150 MHz in the TGSS survey

Sandeep Rana<sup>\*</sup>, Jasjeet S. Bagla<sup>†</sup>

*Indian Institute of Science Education and Research Mohali, Knowledge City, Sector 81, Sahibzada Ajit Singh Nagar, Punjab 140306, India*

4 June 2019

## ABSTRACT

We study the angular clustering of point sources in The GMRT (Giant Meter Wave Telescope) Sky Survey (TGSS). The survey at 150 MHz with  $\delta > -53.5^\circ$  has a sky coverage of  $3.6\pi$  steradians, i.e., 90% of the whole sky. We created subsamples by applying different total flux thresholds limit ( $S_{flux} \gg 5\sigma$ ) for good completeness and measured the angular correlation function  $\omega(\theta)$  of point sources at large scales ( $\geq 1^\circ$ ). We find that the amplitude of angular clustering is higher for brighter subsamples, this indicates that higher threshold flux samples are hosted by massive halos and cluster strongly: this conclusions is based on the assumption that the redshift distribution of sources does not change with flux and this is supported by models of radio sources. We compare our results with other low-frequency studies of clustering of point sources and verify that the amplitude of clustering varies with the flux limit. We quantify this variation as a power law dependence of the amplitude of correlation function with the flux limit. This dependence can be used to estimate foreground contamination due to clustering of point sources for low frequency HI intensity mapping surveys for studying the epoch of reionisation.

**Key words:** Cosmology: large-scale structure of Universe, observation, miscellaneous radio continuum: general

## 1 INTRODUCTION

Low frequency observations of radio sources provide unique information about the population of ultra-relativistic electrons in the inter-stellar medium (ISM) of galaxies: synchrotron emission is the primary radiative mechanism at these frequencies (Condon 1992). Emission from ISM in galaxies and AGNs dominates over the expected flux from neutral Hydrogen via the redshifted 21 cm radiation from the early Universe. This constitutes a significant foreground that needs to be characterized and removed in order to study the evolution of neutral Hydrogen in the Universe. In particular these extragalactic foregrounds affects studies of the epoch of reionisation (EoR) where the inter-galactic medium transitions from being neutral to almost completely ionized (Di Matteo et al. 2004; Liu et al. 2009; Jélic et al. 2008; Trott et al. 2012; Murray et al. 2017; Spinelli, Bernardi, & Santos 2018; Bowman et al. 2018). Redshifted 21 cm radiation from this epoch is likely to be observed at wavelengths in the range 1.5 – 4 m (frequency in the range 75 – 200 MHz). Therefore, a study of point sources and their clustering in this range of frequencies is relevant not just from the per-

spective of studying radio populations but also for its impact on EoR studies. Studies of radio source clustering beyond angular correlation function requires information about redshift, which is not available for an overwhelming majority of sources at present.

A number of studies have been carried out to quantify the faint source population and their clustering at low frequencies. A list of existing and ongoing radio surveys is presented in Table 1.

The Giant Metrewave Radio Telescope (GMRT) was used to survey the radio sky at 150 MHz between 2010 and 2012<sup>1</sup>. Alternative Data Release (ADR1) (Intema et al. 2017) of the TGSS survey contains a catalog of point sources. Here, TGSS data has been analyzed using the SPAM (Source Peeling and Atmospheric Modeling) pipeline, which includes corrections for direction-dependent ionospheric phase effects. Included in ADR1 are continuum stokes I images of 99.5% of the radio sky north of  $\delta = -53^\circ$  ( $3.6\pi$  sr, or 90% of the full sky) at a resolution of  $25'' \times 25''$  north of  $\delta = 19^\circ$  and  $25'' \times 25'' / \cos(\delta - 19^\circ)$  south of  $\delta = 19^\circ$ , with a me-

<sup>\*</sup> E-Mail: sandeep@iisermohali.ac.in

<sup>†</sup> E-Mail: jasjeet@iisermohali.ac.in

<sup>1</sup> Proposal for the survey was made by Sandeep Sirothia, Nimisha Kantharia, Ishwara Chandra and Gopal Krishna (GTAC Cycle 18).

**Table 1.** Low frequency sky surveys. This table enumerates sky surveys at low frequencies. Their sky coverage, sensitivity, frequency and resolution are listed here.

Survey	Frequency(MHz)	Resolution	Noise (mJy beam <sup>-1</sup> )
VLSS(Cohen et al. (2007))	74	80''	100
VLSSr(Lane et al. (2014))	73.8	75''	100
8C(Rees (1990))	38	4.5' × 4.5' csc(δ)	200 – 300
7C(Pooley et al. (1998))	151	70'' × 70'' csc(δ)	20
MSSS-LBA(Heald et al. (2015))	30 – 78	≤ 150''	≤ 50
MSSS-HBA(Heald et al. (2015))	120 – 170	≤ 120''	≤ 10 – 15
TGSS Intema et al. (2017)	150	25''	5
GLEAM(Hurley-Walker et al. (2017))	72 – 231	100''	10
LoTTS(Shimwell et al. (2017))	120 – 168	25''	0.5

dian noise of 3.5 mJy beam<sup>-1</sup>. ADR1 also provides a catalog of radio sources with coordinates, flux density and sizes for 0.62 million sources down to a 7  $\sigma$  peak-to-noise threshold<sup>2</sup>. The data analysis pipeline and data products are described in detail in Intema et al. (2017).

The survey sensitivity for about 80% of the sky covered by TGSS is 5 mJy beam<sup>-1</sup> or better (see figure 8 of Intema et al. (2017)). The estimation of the TGSS confusion noise at 150 MHz and with a 25'' beam ranges between 0.44 mJy beam<sup>-1</sup> and 2.5 mJy beam<sup>-1</sup> for most of the sky. The TGSS point source survey has 50% completeness at 25 mJy (or 7 $\sigma$  for point sources, with  $\sigma$  being the median survey noise of 3.5 mJy beam<sup>-1</sup>). For more detail see Intema et al. (2017). We choose to work with subsets with peak flux thresholds > 32 mJy cutoff to ensure better completeness.

## 2 ANALYSIS AND RESULTS

### 2.1 Survey Selection

Our main aim here is to do study clustering of point sources. We require a sample that is homogeneous and complete for this purpose. The ADR1 data provides the peak flux, source flux and noise on the individual sources. We created a pixelised all-sky map for all sources in TGSS ADR1 catalog with  $N_{side} = 1024$ . This corresponds to mean spacing of 0.057°, using Healpy the python version of HEALPix<sup>3</sup> (Górski et al. 2005). The mean spacing between pixels is much larger than the nominal resolution of 0.0069° but much smaller than the primary beam. We mask out the region  $|b| \leq 10^\circ$  in order to avoid contamination from galactic sources. We also mask out regions of the sky that cannot be observed using the GMRT, i.e.,  $\delta \leq -53^\circ$ . We then mask all pixels with noise level of > 4 mJy beam<sup>-1</sup>. Sources in the remaining pixels can potentially be used for further studies. A binary mask that allows the remaining pixels is also used for generating random catalogs. To study clustering of radio sources, we now create a catalog for sources with peak flux > 32 mJy beam<sup>-1</sup> after imposing the same binary mask. We consider this as the master catalog from where subsets are generated for clustering analysis. We created different

source population subsets with flux threshold using total source flux of  $\geq 50$  mJy, 60 mJy, 100 mJy and 200 mJy respectively. The full ADR1 catalog is 90% complete at total source flux of 60 mJy, with our cut of 4 mJy beam<sup>-1</sup>, we expect better completeness at lower flux thresholds. In order to ensure completeness, we do not use the catalog with a peak flux of 32 mJy beam<sup>-1</sup> but use higher flux thresholds instead. The total number of source in each subset are 267752, 239993, 163654, and, 87751 respectively.  $S \geq 60$  mJy at 150 MHz corresponds to NVSS  $S \geq 10$  mJy, according to the typical spectral index relation (Tiwari 2016; Intema et al. 2017):

$$\alpha_{obs} = \frac{(\log S_{TGSS} - \log S_{NVSS})}{(\log \nu_{NVSS} - \log \nu_{TGSS})} \quad (1)$$

Where  $\nu_{NVSS} = 1.4$  GHz,  $\nu_{TGSS} = 150$  MHz and  $S_{TGSS}$  and  $S_{NVSS}$ , respectively, at the flux densities measured by the TGSS and NVSS for sources common in the two catalogs. We used  $\alpha_{obs} = 0.76$  for conversion (see figure 2 of Tiwari (2016) for details).

Two sky maps are included as online only supplementary material. One map shows the regions with *rms* noise below 4 mJy beam<sup>-1</sup> and the second map shows all the sources in the 50 mJy catalog.

### 2.2 Angular Correlation Function

The angular correlation function  $\omega(\theta)$  describes the clustering of sources on the sky. It is a measure of the excess number of neighboring sources at a separation  $\theta$  on an average, where the excess is measured over a random distribution of sources with the same number density (Peebles 1980). We calculate  $\omega(\theta)$  using the Landy-Szalay (Landy & Szalay 1993) estimator which takes the edge corrections (Kerscher et al. 2000) into account. The angular correlation function is defined in terms of pair counts in the data and the random catalog:

$$\omega(\theta) = \frac{N_r(N_r + 1)DD}{N_d(N_d + 1)RR} - N_d(N_r + 1)\frac{DR}{RR} + 1 \quad (2)$$

Here,  $DD$  denotes the count of pairs in the data at angular separation  $\theta$ , and  $N_d$  is the total number of objects in the data considered in the analysis. Similarly,  $RR$  is the averaged pair count over a catalog of uniformly distributed points covering the same survey area,  $DR$  is the data-random cross pair count, and  $N_r$  denotes the number of points in the random catalog.

<sup>2</sup> <http://tgssadr.strw.leidenuniv.nl/doku.php>

<sup>3</sup> <http://healpix.sourceforge.net>

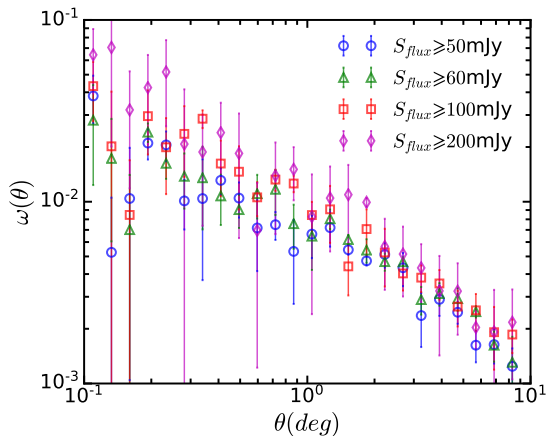


**Figure 1.** Angular correlation function for the four subsets. We see that there is a break in the shape at an angle of  $1^\circ$  with a power law decline at larger scales and a gentler variation at smaller scales. The amplitude of angular correlation is larger for subsamples with a high flux threshold, i.e., brighter sources cluster more strongly.

We created a random catalog for clustering analysis using the survey selection function as described in the previous section.

To compute  $DD$ ,  $RR$  and  $DR$  efficiently, we use the publicly available KD-tree routines (Scikit-learn (Pedregosa et al. 2011)) which are an implementation of spatial algorithms such as kd-tree for fast nearest neighbor search (Bentley 1975; Omohundro 1989). We used the Jackknife re-sampling method (Feigelson & Babu 2012; Andrae 2010), with 200 subsamples drawn randomly from the flux limited data to estimate errors in  $\omega(\theta)$ . In this work, all the plots were produced with MATPLOTLIB Hunter (2007) and frequently used scientific libraries such as NUMPY and SCIPY (van der Walt, Colbert & Varoquaux 2011; Jones, et al. 2001).

We find that the amplitude of the angular correlation function varies monotonically with the flux cut-off at all scales, as shown in Figure 1. As the flux threshold is increased, the amplitude of angular correlation function at a fixed angle increases. This is consistent with findings in earlier studies, e.g., (Peacock & Nicholson 1991; Rengelink 1999; Magliocchetti et al. 2017). This may arise from the known correlation between the star formation rate and the stellar mass of galaxies, e.g., (Lara-López et al. 2013). It is well known that stellar mass and halo masses of galaxies are correlated and higher mass halos are more strongly biased. This may also result from a higher prevalence of AGN in more massive galaxies. While not all high mass galaxies are AGNs, more powerful AGNs are to be found mostly in high mass galaxies and hence are likely to be more strongly biased. Qualitatively we expect this to be true for radio loud AGNs as well (Rengelink 1999; Overzier et al. 2003). Given the flux range, the majority of sources in our sample are expected to be AGNs.

To quantify the shape of the angular correlation function, we assume a power law of the form:  $A\theta^{-\gamma}$  (Cress et al.

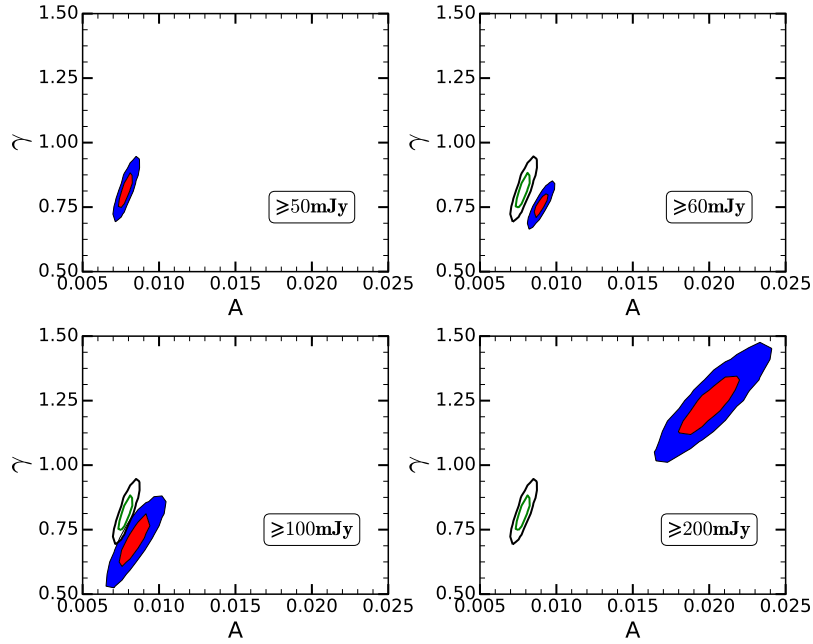
1996; Rengelink 1999; Magliocchetti et al. 1998; Blake & Wall 2002; Overzier et al. 2003; Blake et al. 2004). Here  $A$  is the amplitude,  $\theta$  is the angle in degrees and  $\gamma$  is the power law index. We estimate the posterior probability distribution alongside best fit for amplitude  $A$  and power law index  $\gamma$ . We use the *emcee* package (Foreman-Mackey et al. 2013), which is a Python implementation of MCMC sampling for this estimation. We fit the power law to data at angular scales larger than a degree. This allows us to avoid modeling a change of slope seen in some of the subsets at the scale of a degree: the angular correlation function is shallower at smaller angular scales and its slope appears to vary strongly with the flux cutoff. Further, most EoR experiments are sensitive to larger angular scales and hence we focus on these scales<sup>4</sup>

Figure 2 shows the  $1\sigma$  and  $2\sigma$  confidence intervals for the subsamples with different flux cut-off, plotted in the  $A - \gamma$  plane. We see that as the flux cut-off increases, the dominant effect is an increase in  $A$ . The preferred range of  $\gamma$  remains within  $1\sigma$  region for the 50 mJy catalog and it does not show any strong, systematic evolution with the flux cut-off, except for the brightest subset. Such a behavior may be expected if most of the sources belong to the same class.

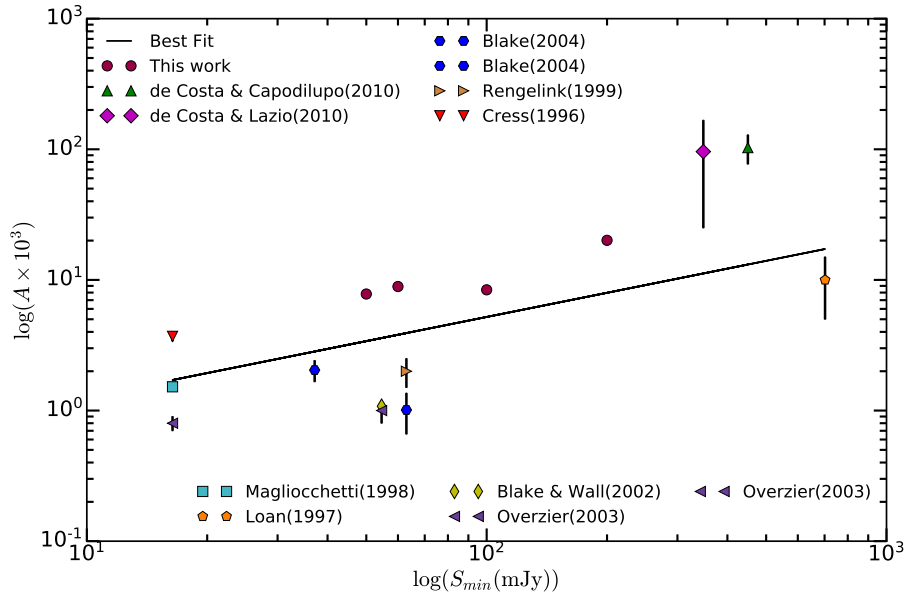
We compare our results with other studies of radio source clustering. In Table 1 we have listed clustering studies of radio sources in surveys carried out at different frequencies (de Oliveira-Costa & Lazio 2010). We find that if we consider surveys with a comparable flux cut-off, as determined by the average spectral index, the amplitude of clustering is comparable within uncertainty. This is illustrated in Figure 3. This figure shows the variation of the amplitude of angular clustering as a function of the scaled flux threshold in different samples assuming a spectral index 0.76. We find that there is a clear trend such that increasing the scaled flux threshold leads to a higher amplitude of clustering. However, we see some scatter around this trend, unlike figure 1 of Rengelink et al. 1999. The source of the scatter is unclear and it may be due to sample variance or the range of angular scales over which a reliable estimation of the angular correlation function can be done in a given sample (Magliocchetti, Bagla, Maddox & Lahav 2000; Blake & Wall 2002; Overzier et al. 2003). Angular resolution can play a role at small angular scales while the extent of the survey on the sky and the geometry can effect the largest scales up to which we can get a reliable estimate of the angular correlation function and not be drowned out by sample/cosmic variance. Another aspect is the use of a single spectral index for scaling observations: variations in the spectral index in different samples can also introduce some scatter.

The line plotted in the top panel of Figure 3 is the best fit power law for these data points and has the form  $a \times 10^{-3} + b \log(S_{min}/(1 \text{ mJy}))$ . The fit is driven by points with smaller error bars. Figure 4 shows the confidence levels of the power law fit. There is no significant variation in the index  $\gamma$  of the angular correlation function with flux limit

<sup>4</sup> For reference, the estimated slope and amplitude if we work with the range  $0.1^\circ \leq \theta \leq 10^\circ$  is shown in a separate figure available online in supplementary material. As can be seen, the slope for the full range of scales is much smaller for all the sets, as is the amplitude. This shows that the slope at smaller angular scales is gentler for all the subsamples.



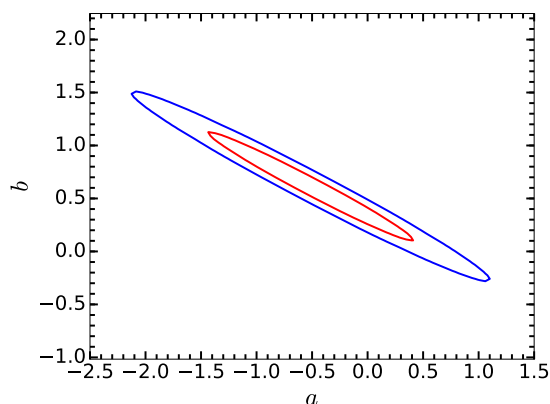
**Figure 2.** Posterior probability distribution for  $A$  and  $\gamma$  using angular correlation data for different flux cut-off values. This is shown for the four subsets.  $1\sigma$  and  $2\sigma$  contours are shown here. The outline of contours for the 50 mJy subset is shown in all the panels for reference. Note that the power law is fit only at scales  $\theta \geq 1^\circ$ .



**Figure 3.** We show the amplitude of correlation function as a function of the scaled flux threshold from different studies. See text for details of the scaling procedure. We find a trend of a higher correlation amplitude for a higher flux threshold. The line plotted in the top panel is the best fit power law for these data points of the form  $(a \times 10^{-3} + b \log(S_{min}/(1 \text{ mJy})))$ . The values are:  $a = -0.51 \pm 0.59$  and  $b = 0.61 \pm 0.33$ , as compared to the values reported earlier:  $a = 0.16 \pm 0.18$  and  $b = 0.35 \pm 0.13$ .

**Table 2.** Best fit value of  $\omega(\theta)$  at low frequencies from current study and earlier published work.

Survey	Ref	$\nu$ (MHz) Sources	$S_{lim}$ (mJy)	$A$ ( $\times 10^{-3}$ )	$\gamma$	Number of	Scaled flux at 150 MHz (mJy)
TGSS	This Work	150	$\geq 50$	$7.8 \pm 0.4$	$0.821 \pm 0.072$	267752	50
TGSS	This Work	150	$\geq 60$	$8.9 \pm 0.5$	$0.760 \pm 0.053$	239993	60
TGSS	This Work	150	$\geq 100$	$8.4 \pm 0.1$	$0.716 \pm 0.104$	163654	100
TGSS	This Work	150	$\geq 200$	$20.1 \pm 0.2$	$1.24 \pm 0.132$	87751	200
VLSS	<a href="#">de Oliveira-Costa &amp; Capodilupo (2010)</a>	74	770	$103 \pm 26$	$1.21 \pm 0.35$	68311	450.1
MIYUN	<a href="#">de Oliveira-Costa &amp; Lazio (2010)</a>	232	250	$96 \pm 71$	$1.12 \pm 0.11$	34426	348.2
PMN	<a href="#">Loan et al. (1997)</a>	$4.85 \times 10^3$	50	$10.0 \pm 5.0$	1.8	77856	701.9
WENSS	<a href="#">Rengelink (1999)</a>	325	35	$2.0 \pm 0.5$	0.8	86461	62.9
WENNS	<a href="#">Blake et al. (2004)</a>	325	35	$1.01 \pm 0.35$	$1.22 \pm 0.33$	86461	62.9
SUMMS	<a href="#">Blake et al. (2004)</a>	843	10	$2.04 \pm 0.38$	$1.24 \pm 0.16$	68373	37.1
FIRST	<a href="#">Cress et al. (1996)</a>	1400	3	$3.7 \pm 0.3$	$1.06 \pm 0.03$	109873	16.4
FIRST	<a href="#">Magliocchetti et al. (1998)</a>	1400	3	$1.52 \pm 0.06$	$1.68 \pm 0.07$	86074	16.4
NVSS	<a href="#">Blake &amp; Wall (2002)</a>	1400	10	$1.08 \pm 0.09$	$0.83 \pm 0.05$	522341	54.6
NVSS	<a href="#">Overzier et al. (2003)</a>	1400	3	$0.8 \pm 0.1$	0.8	210530	16.4
NVSS	<a href="#">Overzier et al. (2003)</a>	1400	10	$1.0 \pm 0.2$	0.8	433951	54.6


**Figure 4.** We show confidence level intervals of the power law fit in the amplitude ( $a$ ) and index ( $b$ ) space.

in our sample at lower flux levels. Thus, the fitted variation of the amplitude of angular clustering can be used for simulations of point source foregrounds at and around 150 MHz. Indeed, this allows for an approach that is independent of the modeling of different types of radio sources ([Di Matteo et al. 2004](#); [Jélic et al. 2008](#); [Liu et al. 2009](#); [Trott et al. 2012](#); [Murray et al. 2017](#)).

Clustering has been analyzed for deeper surveys, e.g., ([Wilman, Röttgering, Overzier & Jarvis 2003](#)), however such surveys so far have covered a smaller area in the sky and hence are not appropriate for comparison with wide field surveys, except perhaps for studying clustering at sub-degree scales.

### 3 DISCUSSION

We discuss our results in the context of source populations and the implications for foreground characterization.

A number of models for radio sources have been developed ([Massardi, Bonaldi, Negrello, Ricciardi, Raccanelli & de Zotti 2010](#); [Mancuso, et al. 2017](#); [Bonato, et al. 2017](#); [Prandoni 2018](#); [Bonaldi, et al. 2019](#)). While early models were largely phenomenological, improvement in multi-wavelength observations have led to development of more sophisticated and realistic models. These models suggest that at low frequencies and at flux ranges of interest, the data sets are dominated by radio loud AGNs. Indeed, at 150 MHz, steep spectrum sources account for nearly the entire source population at fluxes relevant for our dataset ([Massardi, Bonaldi, Negrello, Ricciardi, Raccanelli & de Zotti 2010](#); [Mancuso, et al. 2017](#)). As we go to fainter fluxes, we probe sources at a slightly higher redshifts though the shift is very small compared with the range of redshifts over which the sources are distributed ([Massardi, Bonaldi, Negrello, Ricciardi, Raccanelli & de Zotti 2010](#); [Mancuso, et al. 2017](#)). The fact that we probe primarily one class of sources is the likely reason for the observed variation of clustering amplitude with flux as in [Overzier et al. \(2003\)](#). The observed source population in TGSS consists mostly of AGNs and as brighter AGNs reside in more massive halos, we expect these to be more strongly biased ([Overzier et al. 2003](#); [Magliocchetti et al. 2017](#)). We are analyzing this in detail by combining source population models with models for evolution of bias. Results of the study will be reported in a forthcoming manuscript. Preliminary analysis suggests that at lower fluxes, below 1 mJy at 150 MHz, star forming galaxies begin to contribute significantly and the variation of clustering with flux should change character and deviate from the

power law behavior seen here (Wilman, Röttgering, Overzier & Jarvis 2003).

The quantitative analysis of point source clustering can be used as an input for foreground removal (Murray et al. 2017; Murray, Trott & Jordan 2018). Essentially, the foreground removal methods result in separation of different contributions and an independent assessment of the foregrounds can be used as a calibrator for the foreground removal process. Bright point sources can be removed explicitly and hence a statistical approach is required only for the fainter sources. Smaller amplitude of angular clustering for fainter sources is hence significant in that foregrounds due to clustering of faint sources may be less important than estimated from bright samples. We expect that EoR surveys should be able to remove sources brighter than about 0.1 mJy and hence it is important to estimate angular clustering for fainter radio source populations. However, as we gradually work towards this sensitivity, it is essential to work with the data sets available and refine algorithms. Studies of clustering of sources over a wide range in fluxes allow us to validate models for source populations and their clustering; this is essential if we are to understand and work around foregrounds for the sensitive EoR surveys.

#### 4 SUMMARY

In this paper we have studied the angular clustering of radio sources in the TGSS survey using the catalogs derived in the alternative data release. We have defined our main sample and sub samples using the rms noise and peak flux. We have studied angular clustering of these sources our main results are:

(i) The angular correlation function is a power law at scales larger than a degree: correlation drops rapidly at larger angular separations.

(ii) The angular correlation at scales smaller than a degree has a weaker dependence on scale as compared to larger scales. This is illustrated in a figure available online as supplementary material.

(iii) The slope of the angular correlation function shows little variation with the flux of sources.

(iv) The amplitude of the power law increases monotonically with the peak flux of sources. This is consistent with earlier studies, (Peacock & Nicholson 1991; Rengelink 1999; Wilman, Röttgering, Overzier & Jarvis 2003; Overzier et al. 2003; Magliocchetti et al. 2017).

(v) We have compared our results with other studies of angular clustering of radio sources. We show that assuming a typical spectral index of  $\alpha = 0.76$ , the amplitude of angular clustering is insensitive to the frequency at which the sources are observed and selected. This is in agreement with Rengelink (1999).

(vi) We provide a fit to the variation of the amplitude of clustering with the flux cutoff at 150 MHz. This is potentially useful for modeling of point source foregrounds for EoR studies.

#### ACKNOWLEDGMENTS

Authors thank Manuela Magliocchetti and Nirupam Roy for useful comments and suggestions. We also thank Gianfranco de Zotti for clarifications on models of radio sources. We thank the anonymous reviewer for detailed comments. Authors thank Thilo Max Siewert for pointing out an error in Figure 3 and Figure 4 in the published version. The authors acknowledge the use of the HPC facility at IISER Mohali for this work. This research has made use of NASA's Astrophysics Data System Bibliographic Services.

#### REFERENCES

- Górski K. M., Hivon E., Banday A. J., Wandelt B. D., Hansen F. K., Reinecke M., M. B., 2005, *The Astrophysical Journal*, 622, 759
- Andrae R., 2010, ArXiv e-prints
- Baugh C., Efstathiou G., 1993, *Monthly Notices of the Royal Astronomical Society*, 265, 145
- Bentley J. L., 1975, *Commun. ACM*, 18, 509
- Blake C., Mauch T., Sadler E. M., 2004, *MNRAS*, 347, 787
- Blake C., Wall J., 2002, *MNRAS*, 337, 993
- Bonaldi A., et al., 2019, *MNRAS*, 482, 2
- Bonato M., et al., 2017, *MNRAS*, 469, 1912
- Bowman J. D., Rogers A. E. E., Monsalve R. A., Mozdzen T. J., Mahesh N., 2018, *Natur*, 555, 67
- Cohen A. S., Lane W. M., Cotton W. D., Kassim N. E., Lazio T. J. W., Perley R. A., Condon J. J., Erickson W. C., 2007, *AJ*, 134, 1245
- Condon J. J., 1992, *ARA&A*, 30, 575
- Cress C. M., Helfand D. J., Becker R. H., Gregg M. D., White R. L., 1996, *ApJ*, 473, 7
- de Oliveira-Costa A., Capodilupo J., 2010, *MNRAS*, 404, 1962
- de Oliveira-Costa A., Lazio J., 2010, ArXiv e-prints
- Di Matteo T., Ciardi B., Miniati F., 2004, *Monthly Notices of the Royal Astronomical Society*, 355, 1053
- Efstathiou G., Bernstein G., Tyson J. A., Katz N., Guhathakurta P., 1991, *ApJ*, 380, L47
- Feigelson E. D., Babu G. J., 2012
- Foreman-Mackey D., Hogg D. W., Lang D., Goodman J., 2013, *PASP*, 125, 306
- Heald G. H., Pizzo R. F., Orrú E., Breton R. P., Carbone D., Ferrari C., Hardcastle M. J., 2015, *A&A*, 582, A123
- Hunter J. D., 2007, *Computing in Science & Engineering* 9, 90
- Hurley-Walker N., Callingham J. R., Hancock P. J., Franzen T. M. O., Hindson L., Kapińska A. D., Morgan J., Offringa A. R., Wayth R. B., Wu C., 2017, *MNRAS*, 464, 1146
- Intema H. T., Jagannathan P., Mooley K. P., Frail D. A., 2017, *A&A*, 598, A78
- Eric Jones, et al. 2001, <http://www.scipy.org>
- Kerscher M., Szapudi I., Szalay A. S., 2000, *The Astrophysical Journal Letters*, 535, L13
- Landy S. D., Szalay A. S., 1993, *ApJ*, 412, 64
- Lane W. M., Cotton W. D., van Velzen S., Clarke T. E., Kassim N. E., Helmboldt J. F., Lazio T. J. W., Cohen A. S., 2014, *MNRAS*, 440, 327
- Limber D. N., 1954, *ApJ*, 119, 655

- Liu A., Tegmark M., Zaldarriaga M., 2009, MNRAS, 394, 1575
- Loan A. J., Wall J. V., Lahav O., 1997, MNRAS, 286, 994
- Lara-López M. A., et al., 2013, MNRAS, 434, 451
- Magliocchetti M., Maddox S. J., Lahav O., Wall J. V., 1998, MNRAS, 300, 257
- Magliocchetti M., Bagla J. S., Maddox S. J., Lahav O., 2000, MNRAS, 314, 546
- Magliocchetti M., Popesso P., Brusa M., Salvato M., Laigle C., McCracken H. J., Ilbert O., 2017, MNRAS, 464, 3271
- Mancuso C., et al., 2017, ApJ, 842, 95
- Massardi M., Bonaldi A., Negrello M., Ricciardi S., Raccanelli A., de Zotti G., 2010, MNRAS, 404, 532
- Murray S. G., Trott C. M., Jordan C. H., 2017, The Astrophysical Journal, 845, 7
- Murray S. G., Trott C. M., Jordan C. H., 2018, Peering towards Cosmic Dawn, 199, IAUS..333
- van der Walt, S. and Colbert, S. C. and Varoquaux, G., 2011, arXiv:1102.1523
- Omohundro S. M., 1989, Technical report, Five Balltree Construction Algorithms
- Overzier R. A., Röttgering H. J. A., Rengelink R. B., Wilman R. J., 2003, A&A, 405, 53
- Peacock J. A., Nicholson D., 1991, MNRAS, 253, 307
- Pedregosa F., Varoquaux G., Gramfort A., Michel V., Thirion B., Grisel O., Blondel M., Prettenhofer P., Weiss R., Dubourg V., Vanderplas J., Passos A., Cournapeau D., Brucher M., Perrot M., Duchesnay E., 2011, Journal of Machine Learning Research, 12, 2825
- Peebles P. J. E., 1980, *The Large Scale Structure of the Universe*, Princeton University Press, Princeton, USA
- Pooley D. M., Waldram E. M., Riley J. M., 1998, Monthly Notices of the Royal Astronomical Society, 298, 637
- Prandoni I., 2018, Peering towards Cosmic Dawn, 175, IAUS..333
- Rees N., 1990, MNRAS, 244, 233
- Rengelink R., 1999, in Röttgering H. J. A., Best P. N., Lehnert M. D., eds, *The Most Distant Radio Galaxies Clustering evolution in the radio surveys WENSS and GB6*. p. 399
- Schober J., Schleicher D. R. G., Klessen R. S., 2017, MNRAS, 468, 946
- Shimwell T. W., Röttgering H. J. A., Best P. N., Williams W. L., Dijkema T. J., de Gasperin F., Hardcastle M. J., Heald G. H., 2017, A&A, 598, A104
- Simon P., 2007, A&A, 473, 711
- Spinelli M., Bernardi G., Santos M. G., 2018, arXiv, arXiv:1802.03060
- Tiwari P., 2016, ArXiv 1609.01308
- Trott C. M., Wayth R. B., Tingay S. J., 2012, ApJ, 757, 101
- Wilman R. J., Röttgering H. J. A., Overzier R. A., Jarvis M. J., 2003, MNRAS, 339, 695
- Zehavi I., Zheng Z., Weinberg D. H., Blanton M. R., Bahcall N. A., Berlind A. A., Brinkmann J., Frieman J. A., Gunn J. E., Lupton R. H., Nichol R. C., Percival W. J., Schneider D. P., Skibba R. A., Strauss M. A., Tegmark M., York D. G., 2011, ApJ, 736, 59
- Jélic V., Zaroubi S., Labropoulos P., Thomas R. M., Bernardi G., Brentjens M. A., de Bruyn A. G., 2008, MNRAS, 389
- Strateva, I., Ivezić, Ž., Knapp, G. R., Narayanan, V. K., Strauss, M. A., Gunn, J. E., Lupton, R. H., Schlegel, D., Bahcall, N. A., Brinkmann, J., Brunner, R. J., Budavári, T., Csabai, I., Castander, F. J., Doi, M., Fukugita, M., Györy, Z., Hamabe, M., Hennessy, G., Ichikawa, T., Kunszt, P. Z., Lamb, D. Q., McKay, T. A., Okamura, S., Racusin, J., Sekiguchi, M., Schneider, D. P., Shimasaku, K. and York, D., 2001, AJ, 122